Simultaneous softening of Cu_3N phonon modes along the T_2 line under pressure: A first-principles calculation

Wen Yu,[1,2] Jinggeng Zhao,[1] and Changqing Jin[1]
[1]*Institute of Physics, Chinese Academy of Sciences, P.O. Box 603, Beijing 100080, People's Republic of China*
[2]*Physics Department, University of Science and Technology, Beijing, Beijing 100083, People's Republic of China*
(Received 13 July 2005; revised manuscript received 29 September 2005; published 13 December 2005)

Cu_3N band structures and phonon dispersion curves under pressure are calculated using first-principles density functional theory and density functional perturbation theory with the local density approximation by the plane-wave pseudopotential method. The band structures are similar to other full-potential calculations. The indirect band gap is about 0.13 eV and decreases with increasing pressure. Simultaneous softening of the M_3 and R_{25} zone boundary phonon modes was found and the possible associated successive structural phase transitions were discussed. The mode Grüneisen parameters for optic modes were obtained and the frequency versus pressure relationship was well fitted to second-order polynomials. The quadric relationship between the soft-mode frequency and pressure was also well reproduced for the M_3 and R_{25} soft modes. The large difference of the soft-mode-driven transition pressures for the first high-pressure phases of ReO_3 and Cu_3N were also discussed.

DOI: 10.1103/PhysRevB.72.214116 PACS number(s): 62.50.+p, 63.20.Dj, 64.30.+t, 81.05.Je

I. INTRODUCTION

The temperature-induced structural phase transition (SPT) has been found commonly in perovskite structure materials and has been studied extensively. Most of these phase transitions are driven by the so-called "soft-mode" mechanism.[1–4] This concept is built on the assumption that the crystal gets unstable against a particular phonon vibration mode. For some materials, such as $BaTiO_3$, $PbTiO_3$, and $KTaO_3$, the ferroelectric SPTs are driven by the Brillouin zone (BZ) center soft transverse-optical mode.[1] But soft-phonon-driven SPTs were also commonly found at the BZ corners (M_3 and R_{25} modes). This latter mechanism involves rotations of the common structural element the BX_6 octahedron of the perovskite structure (general formula ABX_3). The difference between these two modes lies in the fact that the M_3 mode represents rotation of the adjacent layers in the same direction ($a^0a^0c^+$ in Glazer's notation[5]), while the R_{25} mode represents the rotation in the opposite sense ($a^0a^0c^-$ in Glazer's notation). R_{25} condensation has been found in $SrTiO_3$, $NaWO_3$, $LaAlO_3$, $CsPbCl_3$, $KMnF_3$, and $NaNbO_3$.[4,6–17] Successive phase transitions dictated by R_{25} followed by M_3 modes or vice versa were also found in $KMnF_3$, $NaNbO_3$, $NaWO_3$, and $CsPbCl_3$.[9–17]

More recently, similar phase transitions driven by a completely different variable of the equation of state have been found—namely, pressure-induced soft-mode SPTs. The representative material showing these transitions is ReO_3. It is in fact the simplest material containing BX_6 octahedra. In this structure, the A site is empty and the X atoms occupy the center of the cubic edges forming collinear bonds with two nearest-neighbor B atoms instead of occupying the face-centered cubic close-packed sites. As a consequence, this open crystal structure has many vacant interstitial sites and is suited for the interposition of other elements or compression under high-pressure conditions. Unlike other perovskite compounds, ReO_3 is metallic and the undistorted cubic structure is stable at all temperature under ambient pressure and shows very complicated pressure-induced SPTs. Since the first discovery of the "compressibility collapse" accompanying the second-order SPT in ReO_3 by Razavi *et al.* in 1978,[18] there have been many experimental and theoretical works concerning the P-V relationship,[19] soft phonon at the M zone boundary,[20] pressure-induced phase transitions,[21,22] lattice dynamics,[23] and first-principles electronic structure and phonon calculations.[24,25] The pressure-induced SPTs in ReO_3 show very complex nature from the work of Jørgensen *et al.*[21] involving both M_3 and R_{25} soft modes. Another closely related compound is WO_3. Its cubic structure, however, has never been found and the semiconducting WO_3 contains a distorted oxygen octahedron with off-center metal ion and undergoes several temperature-induced phase transitions.[26] The relation between electronic structure and lattice stability of ReO_3 and related oxides has been discussed extensively by Stachiotti *et al.*[24,25,27]

In contrast to the above mentioned two compounds which have been studied extensively both experimentally and theoretically, the transition metal nitride Cu_3N has been paid little attention except for some work on thin films motivated by its applications in electronic-optical industry.[28,29] The copper nitride film is unstable and will decompose into the constituent elements at temperatures as low as 300 °C.[29] No temperature-induced SPTs have been found for this compound. The crystal structure of Cu_3N is of the anti-ReO_3 type with a simple cubic unit cell of lattice constant ranging from 3.807 to 3.819 Å.[30,31] As shown in Fig. 1, in this structure, Cu atoms occupy the center of the cubic edges forming collinear bonds with two nearest neighbor N anions; this is in contrast with ReO_3 where the O atoms occupy the center of the cubic edges forming collinear bonds with two nearest Re cations. Electronic structure calculation has shown that pure Cu_3N is a narrow gap semiconductor with a small indirect band gap of about 0.23 eV while Cu_3N with Pd interposition exhibits semimetallic behavior.[32] Theoretical calculation also con-

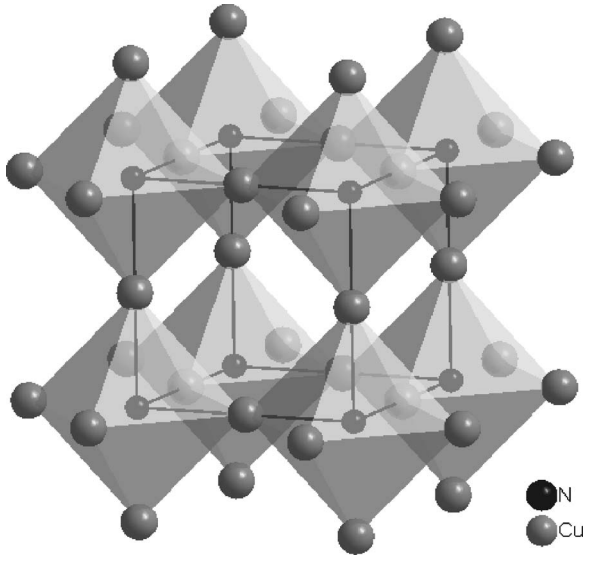

FIG. 1. Schematic view of the anti-ReO_3 crystal structure of Cu_3N structure showing two layers of Cu_6N octahedron.

firmed the metallic property of Cu_3N with extra Cu interposition.[33] To our knowledge, no experimental work has been done on Cu_3N SPTs under high-pressure conditions. In this paper, we hope to investigate the lattice dynamics and possible structural phase transitions for Cu_3N under high-pressure conditions by the first-principles method and compare the results with ReO_3. In view of the fact that ReO_3 is metallic while Cu_3N is semiconducting and its band gap decreases with increasing pressure, it seems an excellent candidate for studying the metallic effect on soft mode transitions.

II. COMPUTATIONAL APPROACH

Our calculations were performed within first-principles density functional theory (DFT) and density functional perturbation theory (DFPT) using the Perdew-Zunger Local density approximation (LDA) exchange-correlation functional and the plane-wave pseudopotential method with three Bessel functions RRKJ-type (introduced by Rappe, Rabe, Kaxiras, and Joannopoulos[34]) ultrasoft pseudopotentials[34] created by Andrea Dal Corso.[35] The electronic wave functions and charge densities were expended in plane-wave basis sets with kinetic energy cutoffs 75 and 450 Ry, respectively. The Brillouin-zone integrations have been performed using a $10\times10\times10$ special k-point set. Phonon frequencies and phonon densities of state were calculated using DFPT with a $4\times4\times4$ Monkhorst-Pack mesh (including the M and R special points) for BZ sampling. Dynamical matrices on this grid have been calculated and the real-space interatomic force constants were given by Fourier deconvolution. The complete phonon dispersion curves were then obtained by interpolating the dynamical matrices using these force constants.

As we were dealing with the case of a narrow gap semiconductor with band gap closing and metallic behavior under pressure, we used Gaussian smearing technique with a smearing parameter. Convergence was checked for different k-point mesh ($4\times4\times4$, $6\times6\times6$, and $8\times8\times8$) and smearing parameters (0.01–0.08 Ry). This gives the phonon frequencies that converge within 1–3 cm^{-1} for positive frequencies. The convergence was a bit poor for the negative (soft) frequencies. We present such a convergence plot for the M_3 soft mode at about 14 GPa in Fig. 2. It can be seen that convergence within 1 cm^{-1} was met for a $4\times4\times4$ k-point mesh with the smearing parameter ranging between 0.01 and 0.04 Ry. Although the k-point convergence seems better for $6\times6\times6$ and $8\times8\times8$ meshes, the convergence with respect to the smearing parameter is poor. Therefore, for efficiency, we chose a $4\times4\times4$ k-point mesh and since Cu_3N is a narrow-gap semiconductor (band gap about 0.13 eV in our calculation), for consistency, we used $\sigma=0.01$ Ry in the whole pressure range.

The structural properties of Cu_3N have been determined by fitting the calculated crystal energies to the Murnaghan

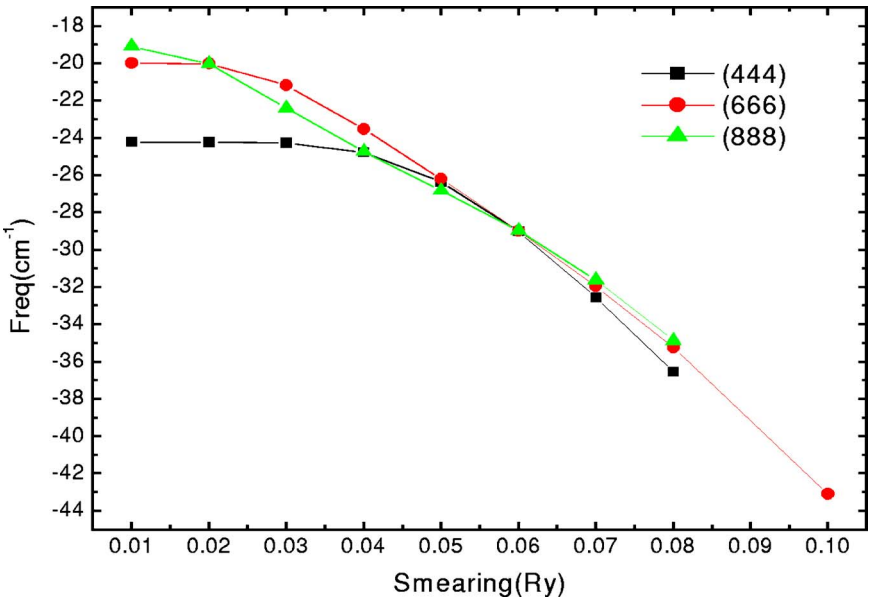

FIG. 2. (Color online) M_3 soft-mode convergence with respect to k-point mesh and smearing at 14 GPa.

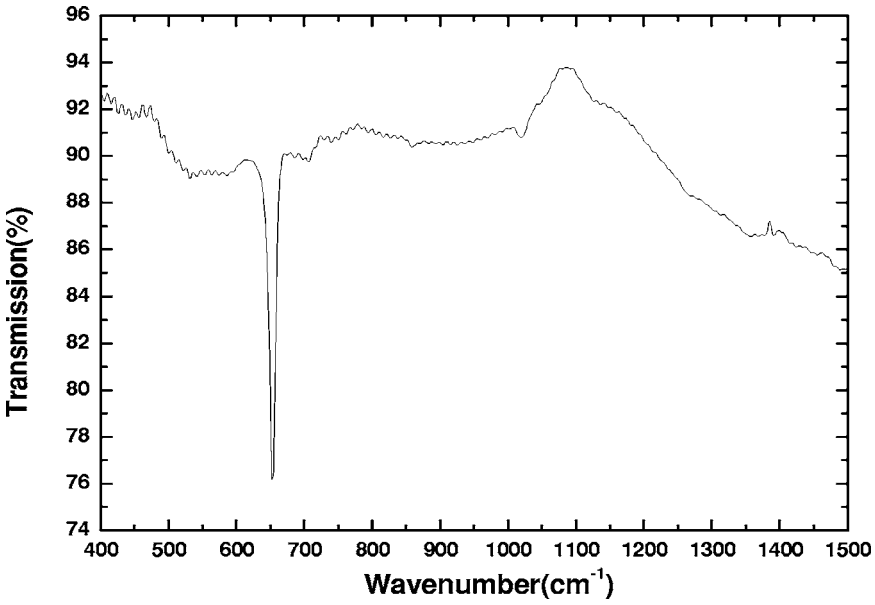

FIG. 3. Infrared transmission spectrum of Cu_3N.

equation of state. The LDA results are compared with the Perdew-Burke-Ernzerhof[36] (PBE) generalized gradient approximation (GGA) and available theoretical and experimental values. Starting from the LDA equilibrium lattice parameter, the phonon dispersion curves of Cu_3N at different compression ratios have been calculated at special points and along the main symmetry lines. The acoustic sum rule and translational invariance were imposed in the calculations. Studies were performed with the PWSCF package.[37]

III. EXPERIMENT

A BIO-RAD FTS60V vacuum infrared spectrophotometer (400–4000 cm^{-1}) was used for the measurement of the infrared spectra at room temperature. Cu_3N powder mixed with KBr (Ratio 1:200) was ground and pressed to form a 0.7-mm-thick slice with a diameter of about 10 mm. A pure KBr slice of the same dimension was also prepared for background.

IV. RESULTS AND DISCUSSION

A. Experiment

The crystal structure of Cu_3N belongs to the space group O_h^1 and the unit cell contains one formula unit. According to space group analysis, there are 12 phonon modes at Γ among which nine are optic modes with symmetry representations $2\Gamma_{15}+1\Gamma_{25}$. The Γ_{15} modes are infrared active and the Γ_{25} modes are optically inactive (silent modes). The observed infrared transmission spectrum in the region 400–1500 cm^{-1} is shown in Fig. 3. In this range, there is a sharp absorbed peak around 652 cm^{-1} corresponding to the Cu-N high-frequency stretching mode Γ_{15}. The calculated frequency for the same mode is about 705 cm^{-1}. It should be pointed out here that the calculated value is at the theoretical minimum energy geometry 3.752 Å. When the experimental lattice constant 3.807 Å was used, the corresponding frequency becomes 651 cm^{-1}, which is in excellent agreement with the experiment. Even at the largest experimental lattice constant 3.819 Å, the calculated frequency 640 cm^{-1} is still acceptable. Restricted by the experimental condition, only one infrared active mode frequency was measured. But the good match is nonetheless an indication of the accuracy of our theoretical approach.

B. Computations

The calculated total energies as a function of volumes were least-squares-fitted to the Murnaghan equation of state. The minimum total energy, the equilibrium lattice constant, and the bulk modulus were readily deduced from the fitted parameters in the equation of state. The calculated lattice constant, bulk modulus, the pressure derivative of bulk modulus, and the frequencies of Cu_3N zone-center optical modes are listed in Tables I and II and compared with available experiments and calculations. The predicted LDA equilibrium lattice constant is 3.752 Å which is 1.6% smaller than the average experiment value 3.813 Å while the GGA value 3.868 Å is 1.4% larger.[30,31] The LDA bulk modulus is about 35% larger than the GGA value and other theoretical predictions. The GGA bulk modulus is in good agreement with the theoretical work using similar exchange-correlation

TABLE I. Equilibrium lattice constant a_0 (Å), bulk modulus B_0(GPa), and pressure derivative of the bulk modulus B_0'. The bulk modulus in parentheses is the GGA result.

	a_0	B_0	B_0'
This work	3.752 (3.868)	141 (108)	4.92 (4.66)
Theory	3.82,[a] 3.817[b]	104[a]	5.26[a]
Expt.	3.807,[c] 3.819[d]		

[a]Reference 33.
[b]Reference 32.
[c]Reference 30.
[d]Reference 31.

TABLE II. Observed (ir) and calculated frequencies (cm^{-1}) of Cu_3N Γ-point optical modes. The values in the parenthesis are calculated at the experimental lattice parameter 3.807 Å.

	Expt.	Theory	Mode
ν_1 (Γ_{15})	652	705 (651)	Cu-N stretching
ν_2 (Γ_{25})		159 (154)	Cu-N-Cu bending
ν_3 (Γ_{15})		100 (99)	Cu-N-Cu bending

functional.[33] No experimental bulk modulus for Cu_3N is available for comparison.

The energy bands at equilibrium lattice constant are displayed in Fig. 4. The band structures are similar to other full-potential calculations. The lowest energy of the conduction band is at the M point while the highest energy of the valence band is at the R point. The indirect band gap is about 0.13 eV which is smaller than experimental and other calculations.[38,32,33] The band gap decreases with decreasing volume and closes at about 6 GPa. Further compression causes the overlap of valance and conduction bands leading to a semimetallic state. In view of the well known fact that LDA underestimates the band gap, the actual band closing pressure should be higher.

With reference to the LDA equilibrium lattice volume, phonon dispersion curves for several values of the crystal residual volume v^* were calculated. The phonon dispersions at the minimum energy geometry along with the phonon density of states are shown in Fig. 5. It can be seen that the low-energy acoustic branch along the M_3-T_2-R_{25} line is rather flat and the low-lying optic branches couple strongly with the acoustic branches. Upon increasing pressure, the frequencies of the optical modes increase steadily and the acoustic M_3 and R_{25} phonons soften simultaneously and eventually condense at different residual volumes. The M_3 mode softens rapidly than the R_{25} mode. The dispersion

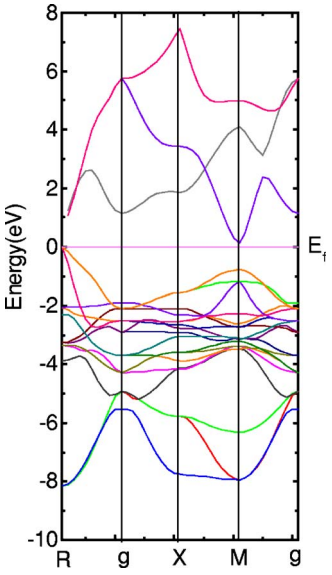

FIG. 4. (Color online) Band structures of Cu_3N along main symmetry lines calculated at equilibrium lattice constant a_0=3.752 Å.

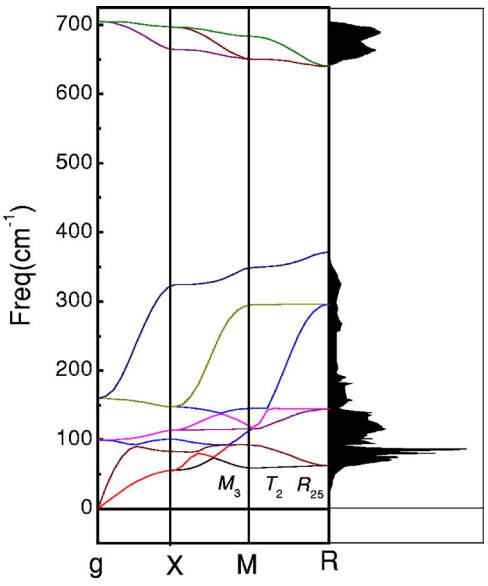

FIG. 5. (Color online) Phonon dispersion curves (with the phonon density of states) calculated at the minimum energy geometry.

curves along with the phonon density of states just above and below the M_3 phonon condensation pressure are given in Fig. 6. The corresponding residual volumes are v^*=0.938 and 0.934 and the pressures are $P^* \approx 10$ and ≈ 11 GPa, respectively. The dispersion curves along with the phonon density of states just above and below the R_{25} phonon condensation are also shown in Fig. 7. The corresponding residual volumes are v^*=0.930 and 0.926 and the pressures are $P^* \approx 12$ and ≈ 13 GPa.

The M_3 mode is nondegenerate and the R_{25} mode is threefold degenerate. Depending on the number of the condensed M_3 phonons in the q-star (one, two, or three), the symmetry-related second-order phase transitions for the perovskite structure could be $Pm3m \rightarrow P4/mbm \rightarrow I4/mmm \rightarrow Im3$. All these structures except $I4/mmm$ were observed for ReO_3 by Jørgensen *et al.*[21] Similarly, the triply degenerate R_{25} soft mode could be treated as made up of three components corresponding to the rotations of the octahedra around three separate [001] axes. If only one component condenses at the transition point, the resulting structure would be of tetragonal symmetry $I4/mcm$ as for $SrTiO_3$ and the coupled condensation of the three components would give a rhombohedral $R3c$ structure which is the case for $LaAlO_3$. When successive phase transitions associated with both M_3 and R_{25} soft modes, the situation becomes complicated and the sequence of phase evolution depends on the condensation sequence of the soft modes. For the case of Cu_3N, since the M_3 phonon condenses first followed by the R_{25} phonon, the first structural transformation would be from cubic $Pm3m$ to tetragonal $P4/mbm$ structure, doubling the unit cell in the plane perpendicular to the rotation axe through one M_3 mode condensation. We are however, unable to determine the subsequent phase evolution solely from the dispersion curves of the cubic structure because of the other remaining M_3 phonons. After the first condensation of one M_3 phonon, the cubic first BZ changes to tetragonal and the M point changes to the Gamma point, the two other M points becomes one A

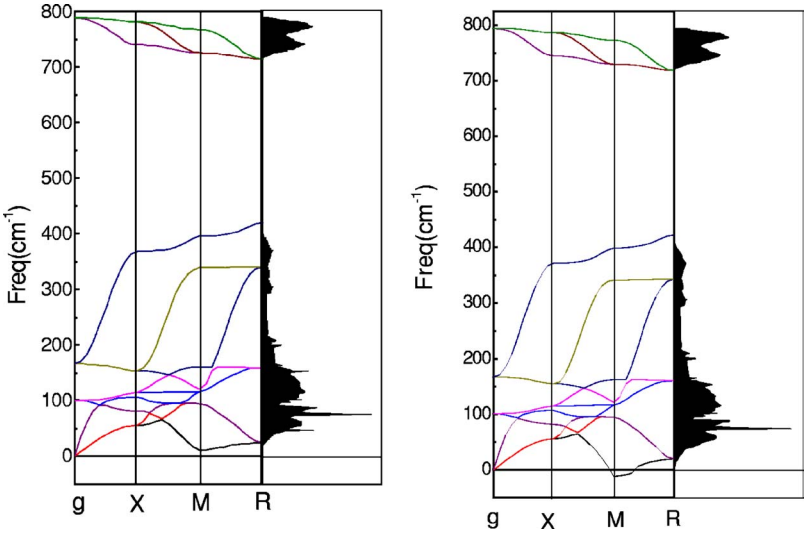

FIG. 6. (Color online) Dispersion curves (with the phonon density of states) just above and below the M_3 phonon condensation pressure (the corresponding residual volumes are $v^*=0.938$ and 0.934 and the pressures are $P^*\approx 10$ and $P^*\approx 11$ GPa, respectively).

point and the R point shifts to the Z point (the triply degenerate R_{25} mode becomes doubly degenerate Z_5 mode). If the twofold degenerate mode from the remaining M_3 phonons condenses successively, the resulting structures would be tetragonal $I4/mmm$ and cubic $Im3$. If coupled condensation occurs, the resulting structure might be orthogonal $Immm$ and $Im3$ depending on the rotation angles around the remaining two cubic axes. If this angle is different from the rotation angle around the first axe, the lattice assumes $Immm$ symmetry. On the other hand, if the two angles equal, the lattice transforms to $Im3$ structure as for ReO_3. However, if the twofold degenerate Z_5 mode condenses successively after the first condensation of the M_3 phonon, the resulting structures would be orthorhombic $Cmcm$ and monoclinic $P2_1/m$ as for $CsPbCl_3$. If the R_{25} condensation occurs after the condensation of all three M_3 phonons, the structural evolution of Cu_3N under pressure might be similar to that of $ReO_3(Pm3m\rightarrow P4/mbm\rightarrow(I4/mmm)\rightarrow Im3\rightarrow(C2/c)\rightarrow R3c)$.[22] It should be pointed out that the $I4/mmm$ structure was not observed by Jørgensen *et al.* and the $C2/c$ space group was not reliably determined due to the lack of resolution.[21] In the paper by Jørgensen *et al.*, a rhombohedral II structure was also found with extremely large bulk modulus even larger than diamond (617 GPa).

Frequencies as a function of pressure for the optic modes are plotted in Fig. 8. From this figure, we can see that the frequencies for the Cu-N-Cu bending modes are almost unchanged with pressure whereas the Cu-N stretching modes increase almost linearly with pressure. More detailed analysis found better agreement with second-order polynomial fitting for all the modes, but all the second order pressure coefficients are very small and decrease with mode frequencies. The effect of pressure on the phonon dispersion curve can be described in terms of the mode Grüeisen parameter, defined as:

$$\gamma_{w_i}=-\frac{\partial \ln \omega_i}{\partial \ln V}=\frac{B_0}{\omega_i}\frac{\partial \omega_i}{\partial P}, \tag{1}$$

where ω_i is the phonon frequency, B_0 is the bulk modulus, V is the crystal volume, and P is the pressure. Using our calculated bulk modulus of $B_0=141$ GPa and the fitted polyno-

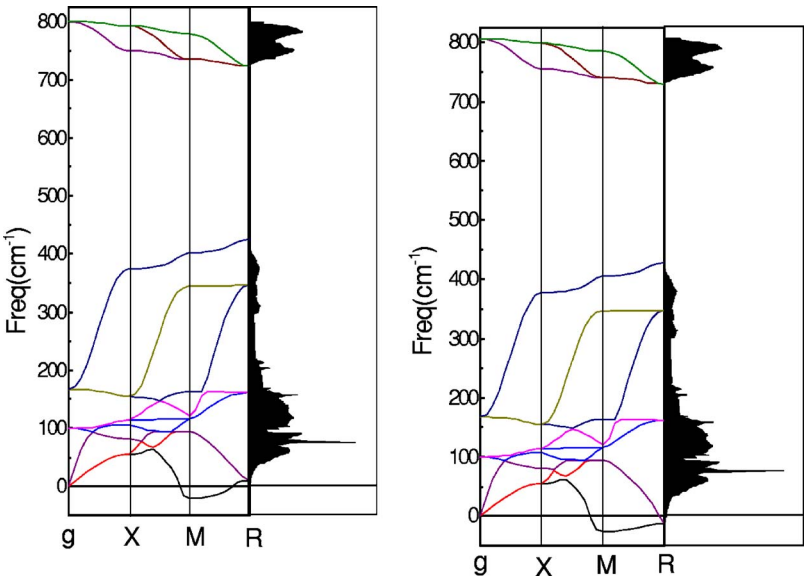

FIG. 7. (Color online) Dispersion curves (with the phonon density of states) just above and below the R_{25} phonon condensation pressure (the corresponding residual volumes are $v^*=0.930$ and 0.926 and the pressures are $P^*\approx 12$ and $P^*\approx 13$ GPa).

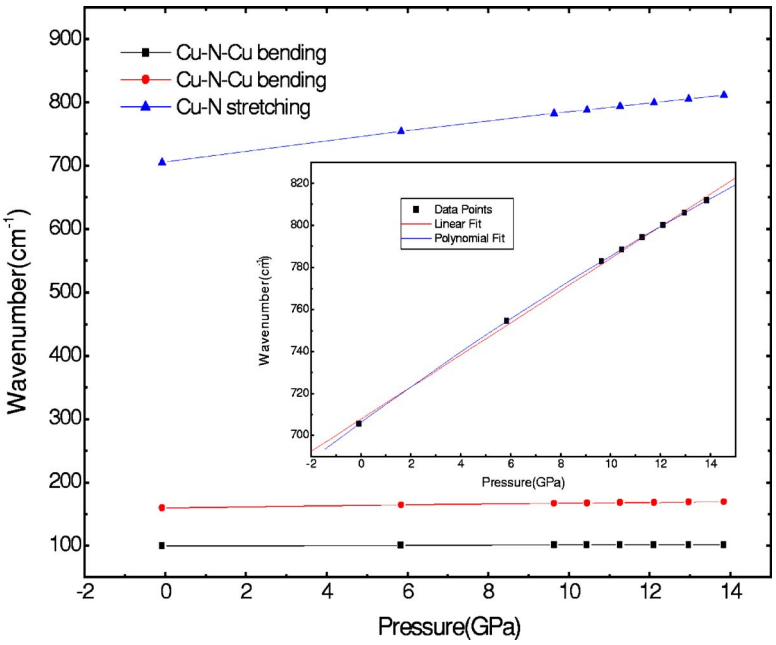

FIG. 8. (Color online) Frequencies as a function of pressure for the Γ-point optic modes Inset: linear and second-order polynomial fitting of the data points for the Cu-N stretching mode.

mial parameters, the zero-pressure mode Grüneisen parameters are 1.74, 0.75, and 0.18 for the Cu-N stretching Γ_{15} and the two Cu-N-Cu bending Γ_{25} and Γ_{15} modes, respectively. Unfortunately, these otherwise measurable mode Grüneisen parameters cannot be measured directly by high pressure Raman scattering study because of the Raman inactivity of the optical modes. For comparison, frequencies as a function of pressure for the M_3 and R_{25} soft acoustic modes are shown in Fig. 9. It can be seen from this figure, the frequencies of these two modes decrease simultaneously with increasing pressure with a pronounced drop near condensation points. The topic of the soft-mode transitions has been discussed extensively and many theories have been proposed to explain the observed effects. One of the common features of "soft mode" behavior is the linear ν^2 versus pressure relationship where ν is the frequency of the soft mode. Except the pressure range close to the softening points, this relationship is well reproduced in our calculation and displayed in Fig. 10.

As mentioned in the Introduction, ReO_3 also shows complex SPTs associated with both M_3 and R_{25} soft modes. The transition pressure for the first phase transition from cubic $Pm3m$ to tetragonal $P4/mbm$ is only 0.5 GPa whereas the calculated first phase transition pressure for Cu_3N is about 10 GPa. This implies that the rotation of the octahedra in Cu_3N is much more difficult than in ReO_3. This is mainly caused by the different bonding mechanism of the metal atoms. In Cu_3N, the Cu atom forms collinear bonds with two nearest N atoms while the Re atom forms octahedra with six O atoms in ReO_3. A detailed description of Cu_3N electronic structure and bonding mechanism has been given by Hahn and

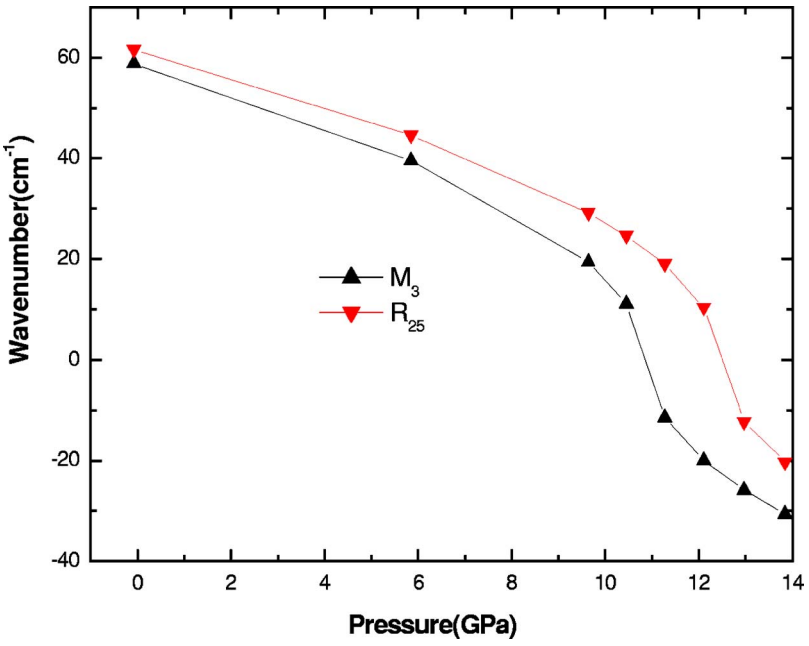

FIG. 9. (Color online) Frequencies as a function of pressure for the M_3 and R_{25} soft acoustic modes.

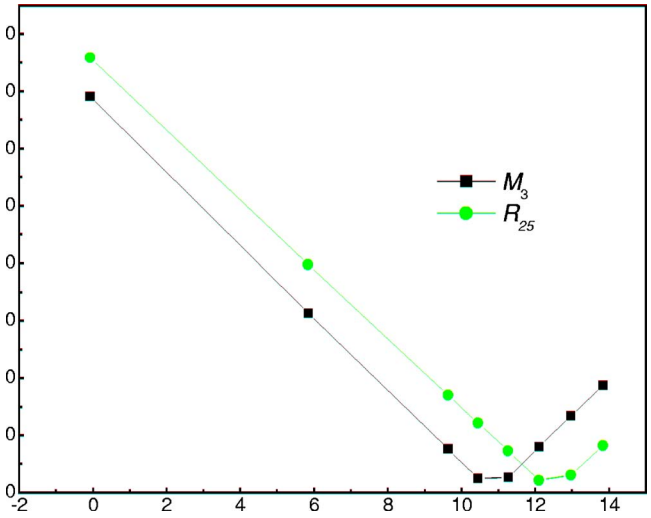

FIG. 10. (Color online) ν^2 versus pressure relationship for the soft M_3 and R_{25} modes.

Weber.[32] The chemical bonding is a mixture of ionic and covalent contributions. Since the valence electronic configurations for Cu and N are $3d^{10}4s$ and $2s^2p^3$ respectively, there are no electrons in the conduction bands of Cu_3N. This is confirmed by the calculated semiconducting property. As can be seen from Fig. 4, the valence band of Cu_3N consists mainly of three parts: three bonding and three anti-bonding Cu $3d$–N $2p$ bands, separated by nonbonding bands. The bonding and anti-bonding bands are asymmetrical with respect to the nonbonding part. The reason for this asymmetry is discussed by the two authors in reference 32 and attributed to the Cu $4s$–N $2p$ coupling leading to a bonding state which otherwise impossible when the bonding and anti-bonding orbitals are fully occupied if only Cu $3d$–N $2p$ hybridization is taken into account. Also pointed out in the reference is the fact that the hybridization of the Cu $4s$ states is more prominent than that of the Cu $4p$ states. But with the decreasing volume, the Cu $4p$–N $2p$ hybridization becomes important which lowers the energy of the conduction band close to the M point as can be seen from Fig. 11 where the conduction band crosses the Fermi level introducing holes in the valence bands and the compound becomes semimetallic. Now it can be augured that under zero pressure, Cu forms dumbbell-like covalent bonds with two nearest N atoms, this covalent bonding prevents the rotation of the octahedra. With increasing pressure, the covalent bond becomes weaker and some metallic contribution comes into effect. This metallic effect eases the rotation of the octahedra and causes the soft mode transition of the M_3 phonon. This is supported by the fact that the semiconductor-semimetal transition pressure is almost coincident with the softening pressure of the M_3 mode. By the same argument, the metallic bonding in ReO_3 might be the main cause of the low phase transition pressure of 0.5 GPa for the first high-pressure phase.

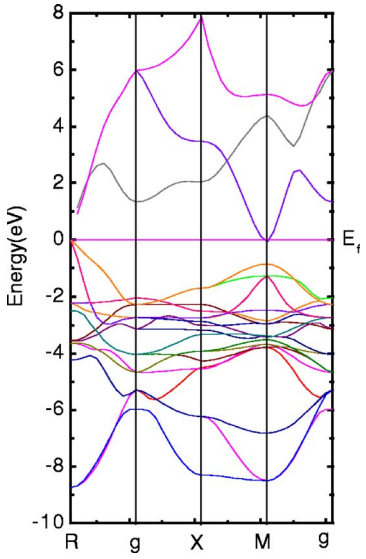

FIG. 11. (Color online) Band structures of Cu_3N along main symmetry lines calculated at residual volume $v^*=0.942$ ($P^*\approx 9.6$ GPa).

V. CONCLUSIONS

In conclusion, we have performed first-principles calculations of the band structures and phonon dispersion curves for Cu_3N at different compression ratios. The band structure is comparable with those obtained in other theoretical works and the band gap decreases with increasing pressure and eventually closes at about 6 GPa. Simultaneous softening of low-energy acoustic modes along the M_3-R_{25} line was observed and the possible structural phase transitions driven by the softening of these two modes were discussed. The mode Grüneisen parameters were calculated for the optical modes and the linear ν^2 versus pressure relationship is well reproduced in our calculation for the two soft acoustic phonon modes. The large difference of the transition pressures for ReO_3 and Cu_3N is discussed and the importance of metallic bonding is pointed out. The "compressibility collapse" and extremely hard rhomohedral II phase found experimentally for ReO_3 deserve further investigation in the case of Cu_3N.

ACKNOWLEDGMENTS

This work was supported by the NSF and Ministry of Science and Technology of China through research projects (No. 50321101, No. 50332020, No. 50328102, No. 2002CB613301, and No. 2005CB724400). One of the authors, W.Y., would like to thank Paolo Giannozzi, Stefano de Gironcoli, Yanming Ma, and all other members of the PWSCF forum for invaluable suggestions and discussions.

[1] W. Cochran, Adv. Phys. **10**, 401 (1961).
[2] J. F. Scott, Rev. Mod. Phys. **46**, 83 (1974).
[3] G. Shirane, Rev. Mod. Phys. **46**, 437 (1974).
[4] J. D. Axe, G. Shirane, and K. A. Müller, Phys. Rev. **183**, 820 (1969).
[5] M. Glazer, Acta Crystallogr., Sect. B: Struct. Crystallogr. Cryst. Chem. **28**, 3384 (1972).
[6] G. Shirane and Y. Yamada, Phys. Rev. **177**, 858 (1969).
[7] R. A. Cowley, Phys. Rev. **134**, A981 (1964).
[8] J. K. Kjems, G. Shirane, K. A. Müller, and H. J. Scheel, Phys. Rev. B **8**, 1119 (1973).
[9] G. Shirane, V. J. Minkiewicz, and A. Linz, Solid State Commun. **8**, 1941 (1970).
[10] V. J. Minkiewicz and G. Shirane, J. Phys. Soc. Jpn. **26**, 674 (1969).
[11] V. J. Minkiewicz, Yasuhiko Fujii, and Yasusada Yamada, J. Phys. Soc. Jpn. **28**, 443 (1970).
[12] K. Gesi, J. D. Axe, G. Shirane, and A. Linz, Phys. Rev. B **5**, 1933 (1972).
[13] F. Denoyer, R. Comes, and M. Lambert, Solid State Commun. **8**, 1979 (1970)
[14] F. Denoyer, R. Comes, and M. Lambert, Acta Crystallogr., Sect. A: Cryst. Phys., Diffr., Theor. Gen. Crystallogr. **27**, 414 (1971).
[15] Roy Clarke, Phys. Rev. Lett. **39**, 1550 (1977).
[16] M. Sato, B. H. Grier, G. Shirane, and T. Akahane, Phys. Rev. B **25**, 6876 (1982).
[17] Y. Fujii, S. Hoshino, Y. Yamada, and G. Shirane, Phys. Rev. B **9**, 4549 (1971).
[18] F. S. Razavi, Z. Altounian, and W. R. Datara, Solid State Commun. **28**, 217 (1978).
[19] B. Batlogg, R. G. Maines, M. Greenblatt, and S. DiGregorio, Phys. Rev. B **29**, 3762 (1984).
[20] J. D. Axe, Y. Fujii, B. Batlogg, M. Greenblatt, and S. DiGregorio, Phys. Rev. B **31**, 663 (1985).
[21] J.-E. Jørgensen, J. D. Jorgensen, B. Batlogg, J. Remeika, and J. D. Axe, Phys. Rev. B **33**, 4793 (1986).
[22] J.-E. Jørgensen, J. Staun Olsen and L. Gerward, J. Appl. Crystallogr. **33**, 279 (2000).
[23] A. P. Mirgorodsky and M. B. Smirnov, J. Phys.: Condens. Matter **5**, 3313 (1993).
[24] F. Corà, M. Stachiotti, and C. Catlow, J. Phys. Chem. B **101**, 3945 (1997).
[25] M. G. Stachiotti, F. Corà, C. R, A. Catlow, and C. O. Rodriguez, Phys. Rev. B **55**, 7508 (1997).
[26] E. Salje, Acta Crystallogr., Sect. B: Struct. Crystallogr. Cryst. Chem. **33**, 547 (1977).
[27] F. Corà, A. Patel, N. Harrison, R. Dovesi, and C. A. Catlow, J. Am. Chem. Soc. **118**, 12174 (1996).
[28] Z. Q. Liu, W. J. Wang, T. M. Wang, S. Chao, and S. K. Zheng, Thin Solid Films **325**, 55 (1998).
[29] T. Maruyama and T. Morishita, Appl. Phys. Lett. **69**, 890 (1996).
[30] R. Juza u. H. Hahn. Z. Anorg. Allg. Chem. **182**, 239 (1938).
[31] U. Zachwiecha and H. Jacobs, J. Less-Common Met. **161**, 175 (1990).
[32] U. Hahn and W. Weber, Phys. Rev. B **53**, 12684 (1996)
[33] M. Moreno-Armenta, A. Martines-Ruiz, and N. Takeuchi, Solid State Sci. **6**, 9 (2004).
[34] A. M. Rappe, K. M. Rabe, E. Kaxiras, and J. D. Joannopoulos, Phys. Rev. B **41**, 1227 (1990).
[35] http://www.pwscf.org/pseudo/1.3/UPF/Cu.pz-d-rrkjus.UPF.
[36] J. P. Perdew, K. Burke, and M. Ernzerhof, Phys. Rev. Lett. **77**, 3865 (1996).
[37] S. Baroni, A. Dal Corso, S. de Gironcoli, and P. Giannozzi, http://www.pwscf.org
[38] J. F. Pierson, Vacuum **66**, 59 (2002).